Molecular Modeling to Increase Kraft Pulp Yield

Cooperative Research and Development Final Report

CRADA Number: CRD-18-00782

NREL Technical Contact: Brandon Knott

NREL is a national laboratory of the U.S. Department of Energy
Office of Energy Efficiency & Renewable Energy
Operated by the Alliance for Sustainable Energy, LLC

This report is available at no cost from the National Renewable Energy Laboratory (NREL) at www.nrel.gov/publications.

Contract No. DE-AC36-08GO28308

Technical Report
NREL/TP-2800-79017
February 2021

Molecular Modeling to Increase Kraft Pulp Yield

Cooperative Research and Development Final Report

CRADA Number: CRD-18-00782

NREL Technical Contact: Brandon Knott

Suggested Citation
Knott, Brandon. 2021. Molecular Modeling to Increase Kraft Pulp Yield*: Cooperative Research and Development Final Report, CRADA Number CRD-18-00782.* Golden, CO: National Renewable Energy Laboratory. NREL/TP- 2800-79017. https://www.nrel.gov/docs/fy21osti/79017.pdf.

NREL is a national laboratory of the U.S. Department of Energy
Office of Energy Efficiency & Renewable Energy
Operated by the Alliance for Sustainable Energy, LLC

This report is available at no cost from the National Renewable Energy Laboratory (NREL) at www.nrel.gov/publications.

Contract No. DE-AC36-08GO28308

Technical Report
NREL/TP-2800-79017
February 2021

National Renewable Energy Laboratory
15013 Denver West Parkway
Golden, CO 80401
303-275-3000 • www.nrel.gov

NOTICE

This work was authored [in part] by the National Renewable Energy Laboratory, operated by Alliance for Sustainable Energy, LLC, for the U.S. Department of Energy (DOE) under Contract No. DE-AC36-08GO28308. Funding provided by U.S. Department of Energy Office of Energy Efficiency and Renewable Energy Advanced Manufacturing Office. The views expressed herein do not necessarily represent the views of the DOE or the U.S. Government.

This report is available at no cost from the National Renewable Energy Laboratory (NREL) at www.nrel.gov/publications.

U.S. Department of Energy (DOE) reports produced after 1991 and a growing number of pre-1991 documents are available free via www.OSTI.gov.

Cover Photos by Dennis Schroeder: (clockwise, left to right) NREL 51934, NREL 45897, NREL 42160, NREL 45891, NREL 48097, NREL 46526.

NREL prints on paper that contains recycled content.

Cooperative Research and Development Final Report

Report Date: January 13, 2021

In accordance with requirements set forth in the terms of the CRADA agreement, this document is the final CRADA report, including a list of subject inventions, to be forwarded to the DOE Office of Scientific and Technical Information as part of the commitment to the public to demonstrate results of federally funded research.

Parties to the Agreement: Alliance for Pulp and Paper Innovation Technology

CRADA Number: CRD-18-00782

CRADA Title: Molecular Modeling to Increase Kraft Pulp Yield

Responsible Technical Contact at Alliance/NREL:

Brandon Knott | Brandon.Knott@nrel.gov

Name and Email Address of POC at Company:

David Turpin | David.Turpin@appti.org

Sponsoring DOE Program Office(s):

USDOE Office of Energy Efficiency and Renewable Energy (EERE), Advanced Manufacturing Office (AMO)

Joint Work Statement Funding Table showing DOE commitment:

Estimated Costs	NREL Shared Resources a/k/a Government In-Kind
Year 1	$150,000.00
TOTALS	$150,000.00

Executive Summary of CRADA Work:

The purpose of this CRADA is to combine industrial expertise in wood pulping with national laboratory expertise in high-performance computer simulation to gain fundamental understanding of softwood pretreatment required to improve the efficiency of kraft pulping.

Summary of Research Results:

The pulp and paper industry is an essential segment of the American economy, making products necessary for everyday life from renewable resources. Kraft pulping, the predominant technology for removing lignin from wood carbohydrates, is energy-intensive, capital-intensive, and provides a less efficient use of wood resources than desired. Wood remains the largest cost in the

manufacture of wood pulp for paper, and increasing pulp yield has the largest financial impact on pulp mill economics. Increasing kraft pulp yield would improve energy efficiency, increase mill profitability, and preserve jobs (this industry employs 378,000 American workers). For example, increasing pulp yield to 50% from the current 45% would decrease the energy intensity by ~10% (13T BTU/year), corresponding to ~$33,000,000, and also reduce carbon emissions.

A 5% yield increase has never been achieved because the alkaline lability of wood carbohydrates promotes peeling reactions wherein sugars are lost ("peeled") from carbohydrate chain ends. Softwood pretreatment with methyl mercaptide (MM) has been demonstrated to increase yield by 3% primarily by stabilizing cellulose against degradation by alkaline peeling (general reaction scheme shown in **Figure 1**). Unfortunately, galactoglucomannan (GGM, the primary hemicellulose molecule in softwood) stabilization by this pretreatment is minimal, and thus represents a promising target for increasing the overall preservation of wood carbohydrates and thus increasing yield.

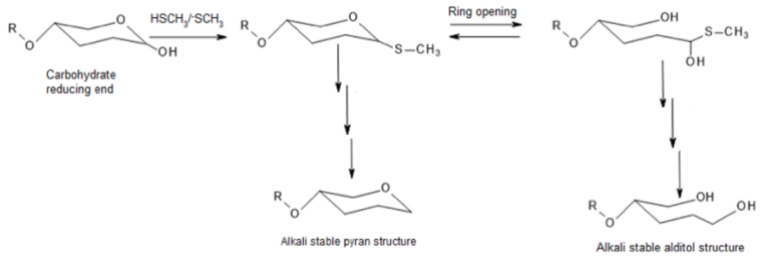

Figure 1. Reducing end group (REG) stabilization by methyl mercaptan.

In the current work, a fundamental understanding of the MM and alkali reactivity of wood components has been elucidated via a multi-pronged molecular modeling approach involving molecular dynamics simulations and density functional theory reaction mechanism calculations. We report reaction pathways and kinetics of pretreatment reactions for model structures representing the biomass polysaccharides GGM and cellulose. Evaluation of the reactivity of these species reveals sites of reaction, thermodynamics, and kinetics, demonstrating how and why the pretreatment chemistry selectively interrupts the peeling reaction for cellulose and how the analogous reactions of native GGM might be controlled. Kinetic data and quantitative product analysis of pretreated real wood chips provided by the University of Maine (PI Adriaan van Heiningen) enable validation and comparison of computational setup and results.

Task 1: Molecular dynamics (MD) simulations of biomass polysaccharides for peeling and pretreatment reactions

Molecular dynamics (MD) simulations are utilized here to determine the spatial distributions of ionic additives of the pretreatment chemistry around each biomass polysaccharide. In addition, MD simulations are used to determine the analogous distributions of the ions that are formed upon dissociation of the active alkaline species that perform peeling reactions (NaOH and Na_2S in aqueous solution). The interactions of these ions have been probed with the unmodified forms of cellulose and hemicellulose as well as with the corresponding forms modified by pretreatment.

MD model construction. To construct the complex model of GGM bound to cellulose, a 36-chain cellulose I_β microfibril model with degree of polymerization (DP) of 20 was first generated with a

diamond cross-sectional geometry. 18 GGM molecules with DP of 15 were then randomly arranged around the cellulose microfibril (**Figure 2B**), resulting in a cellulose/GGM ratio of 2.7, which is consistent with the experimentally observed cellulose/GGM ratio of ~2.6.[1] Our model constructs a GGM molecule as being composed of three repeat units, each consisting of three mannose residues, one glucose residue, and one galactose residue (**Figure 2A**). The galactose residue is attached to the glucose residue at the backbone by α-1,6-linkage. In addition, because cellulose is a simple homopolymer consisting of repeating D-anhydroglucopyranose units linked by β-(1-4)-glycosidic bonds, we used a β-(1-4)-glycosidic bonded glucose dimer (Glu-Glu) to represent the cellulose for additional simulations (and subsequently for QM calculations) (**Figure 2C**). GGM is a heteropolymer consisting of uneven β-(1-4)-linked glucose and mannose as a backbone with some mannose units substituted by α-(1-6)-linked galactose. The molar ratio 'galactose: glucose: mannose' in GGM is approximately 1:1:3. Because of the 1:3 molar ratio between glucose and mannose, we used β-(1-4)-linked mannose dimer (Man-Man) instead of glucose-mannose dimer to represent GGM (**Figure 2C**). These dimer simulations were constructed, along with pretreated forms of Glu-Glu and Man-Man dimers (**Figure 2D**), both for computational efficiency and also to remove supramolecular effects in comparing cellulose to GGM (due to cellulose bundling into microfibrils whereas GGM does not). All generated models were solvated with explicit TIP3P[2] water molecules. Where necessary in all simulations, charge neutrality was achieved by adding sodium cations and hydroxide or thiomethoxide anions.

MD simulation details. All the MD simulations were conducted using CHARMM program[3] with the CHARMM carbohydrate force field, all36_carb.[4-5] The DOMDEC fast parallel CHARMM method[6] was used in the molecular dynamics. All simulations used a 2 fs timestep and SHAKE[7] to keep the length of bonds to hydrogen fixed. Periodic solvated systems used a nonbonded cutoff of 11 Å, with a 2 Å list buffer and heuristic list update using a 1 Å switching function for dispersion, and Particle-Mesh Ewald method[8] for calculating electrostatics accurately to long range. All the systems were equilibrated with initial minimization and 200 ps constant pressure simulations (*NPT*) at 300 K. Subsequently, production runs of 300 ns for GGM/cellulose microfibril complex and 100 ns for varying dimer systems were performed in the *NVT* ensemble.

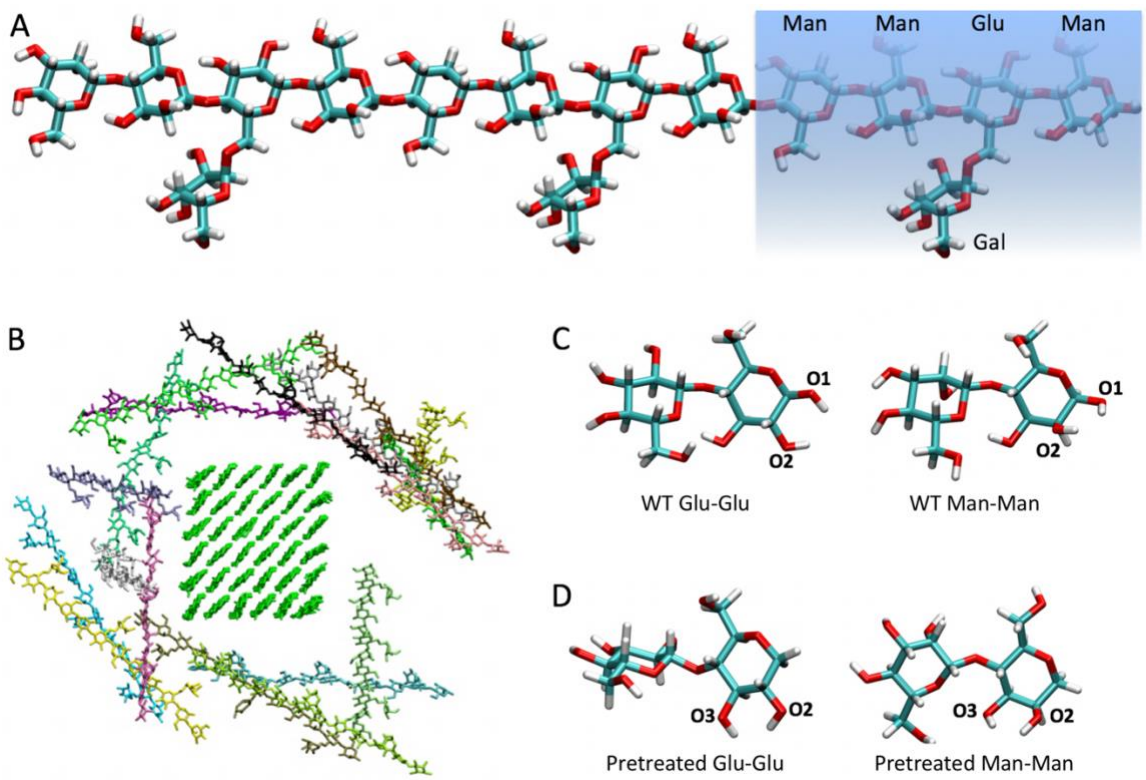

Figure 2. Atomistic models for MD simulation. A) The model of galactoglucomannan (GGM) molecule is composed of three repeating units (one repeat unit shown shaded in blue), each consisting of three mannose residues, one glucose residue, and one galactose residue. B) Edge-on view of a 36-chain cellulose microfibril (center, in green) randomly surrounded by 18 GGM molecules (various colors). This is an example of a starting configuration; following dynamics, some of the hemicellulose molecules bind to the cellulose microfibril (Figure 3). C) Wild type Glu-Glu (glucose dimer) and Man-Man (mannose dimer). Note the difference in orientation of the -OH at the O2 position between glucose and mannose. D) Pretreated Glu-Glu and Man-Man dimers, wherein the O1 hydroxyl is replaced by hydrogen to create an alkaline stable species.

Cellulose/GGM simulations. 300 ns simulation of GGM/cellulose microfibril complex under peeling conditions in the presence of NaOH (**Figure 3A, 3B**) reveals the distribution of OH^- ions (responsible for peeling reactions upon dissociation of NaOH). Simulations at both 0.9 M and 1.5 M NaOH indicate that OH^- ions have a much stronger affinity to bind to the reducing end of GGM than to cellulose (**Figure 3C**). (Affinity here as indicated by the radial distribution functions; thermodynamics were not directly measured.) This difference in affinity could be due to the chemical differences between cellulose and GGM or to the crystalline nature of cellulose possibly rendering physical protection against peeling.

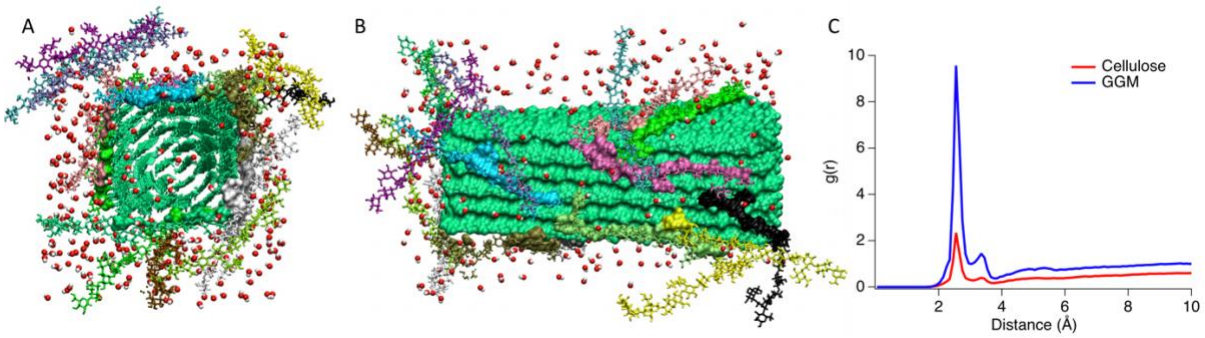

Figure 3. Snapshot of the GGM/cellulose complex at the end of a 300 ns MD simulation. (A) end-on view and (B) side view with cellulose microfibril shown in green surface representation and bound GGM residues shown in solid surface model of various colors. Unbound GGM residues are shown in stick representation. Hydroxide ions are shown as spheres (red: oxygen atoms, white: hydrogen atoms). (C) Radial distribution function of OH^- ions with respect to O1 and O2 at the reducing end of cellulose or GGM. Results shown are with NaOH concentration of 0.9 M; 1.5 M NaOH loading showed qualitatively similar behavior.

Dimer simulations under peeling conditions. The higher affinity of hydroxide ions for GGM than for cellulose (as deduced from radial distribution functions) was also seen in 100 ns simulations of Glu-Glu and Man-Man dimers (**Figure 4**). Glucose and mannose differ only in the stereochemistry at the C2 carbon, and our results demonstrate that OH^- ions exhibit a stronger affinity to localize at the bridging position between the O1-O2 atoms in mannose (**Figure 4C**), possibly promoting more substantial peeling of mannose (and thus in GGM) than glucose even in the absence of supramolecular structure (i.e., cellulose microfibril). Analogous simulations with pretreated dimers indicate that OH^- ions retain a stronger affinity to the hydroxy group in mannose, but now around the O2-O3 atoms (**Figure 4D-F**). This enhanced affinity is possibly due to *cis*-OH groups at these two carbon ring atoms and could promote both the peeling reaction in the WT Man-Man dimer and the dehydration reaction in the pretreated Man-Man dimer. Dehydration occurring at the C3 atom is a precursor reaction that can subsequently trigger the β-hydroxycarbonyl elimination reaction (as illustrated in **Figure 7A**, reaction P3 → P4) to degrade cellulose.

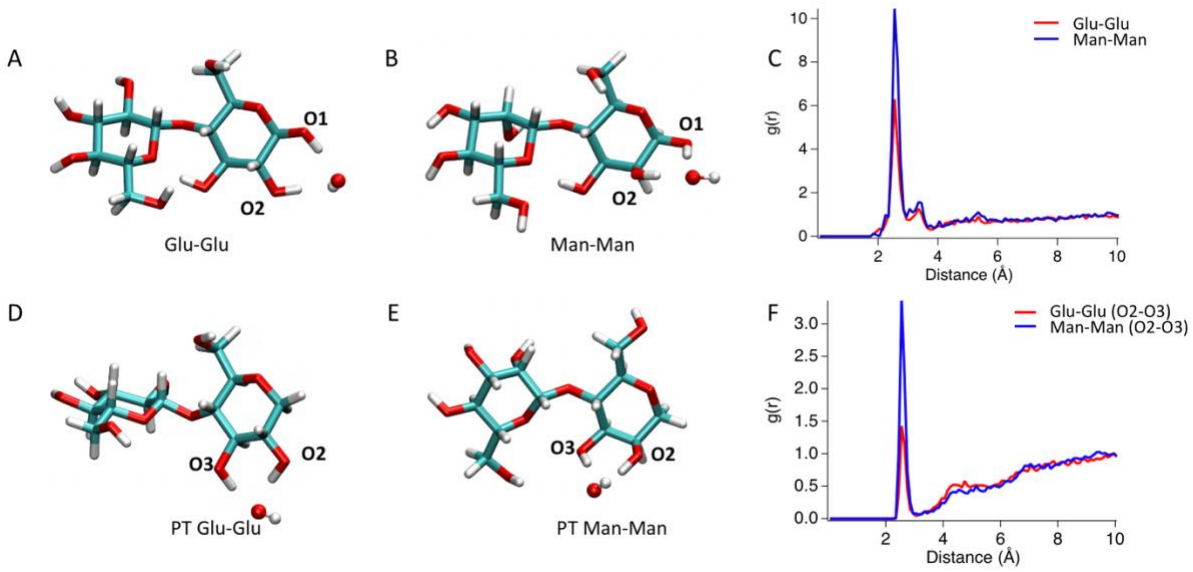

Figure 4. Simulations of Glu-Glu and Man-Man dimers in NaOH solution. Example snapshots of a OH^- ion located at the bridging position between O1 and O2 at the reducing end of (A) a Glu-Glu dimer and (B) Man-Man dimer. (C) Radial distribution function of OH^- ions with respect to O1 and O2 at the reducing end of a Glu-Glu (red) or Man-Man (blue) dimer (NaOH concentration of 1.5 M). Pretreated dimers: (D) PT Glu-Glu and (E) PT Man-Man demonstrate an analogous trend, whereas (F) OH^- prefers the O2-O3 position in PT Man-Man.

Dimer simulations under pretreatment conditions. The final classical MD scenario examined the distribution of CH_3S^- ions that form upon dissociation of sodium methyl mercaptan. These ions perform the pretreatment reactions, and, similar to the hydroxide ions described above, they exhibit affinity for the C1 atom in both Glu-Glu and Man-Man dimers. This position may be favorable for the nucleophilic S_N2 reaction that accomplishes the conversion to alkali stable end group and tends to be slightly higher in glucose than mannose (**Figure 5**).

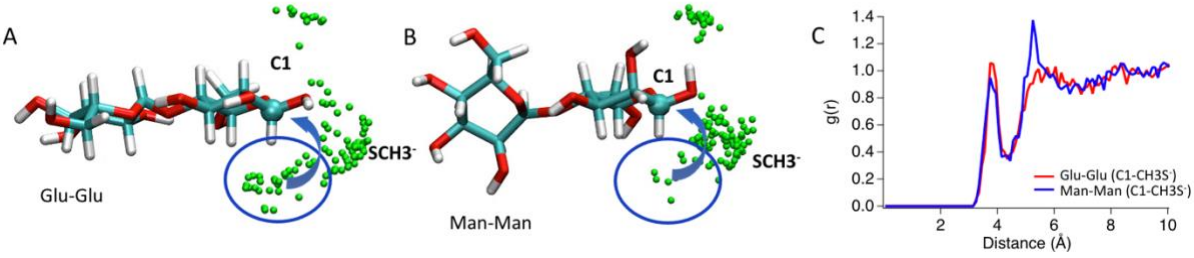

Figure 5. Simulations of pretreated Glu-Glu and Man-Man dimers in NaSCH3 solution. Snapshots of CH3S- ions around C1 at the reducing end of (A) a Glu-Glu dimer and (B) Man-Man dimer. (C) Radial distribution function of CH3S- ions with respect to C1 at the reducing end of a Glu-Glu (red) or Man-Man (blue) dimer (CH3S- concentration of 1.5 M).

Reactive MD under peeling and pretreatment conditions. In addition to purely classical MD simulations, reactive MD simulations at various operating conditions allowed for characterization of reactive configurations for pretreatment and peeling. High-fidelity reactive force fields for the species and operating conditions of interest are not available, but the purpose of these simulations is not a faithful reproduction of reaction energetics. Rather, reactant and intermediate configurations obtained from reactive MD were subsequently examined with density functional

theory (DFT)-based mechanistic studies (described in depth below in Task 2). ReaxFF[9], a reactive forcefield wherein the breaking and forming of chemical bonds (not possible in purely classical MD) is captured, has been developed and applied for a wide range of systems to examine the chemical evolution of these systems at the atomistic level.[10-11]

The ReaxFF MD simulations were conducted to initiate the study of the reaction mechanism for the β-hydroxycarbonyl elimination reaction, i.e., the breaking of β-1,4 bond, using the intermediate P3 of a Glu-Glu dimer shown in **Figure 7A** as the model compound. After testing three different flavors of ReaxFF force fields[12-14], we selected on that demonstrated the tendency to preferentially break β-1,4 bonds before C-C bonds. The system contains 1 Glu-Glu dimer and 21 NaOH, corresponding to a concentration of 2 M NaOH. All reactive simulations were conducted in the *NVT* ensemble at 300 K for 10 ps with a timestep of 0.1 fs. Of the 100 independent ReaxFF MD simulations conducted, 75 revealed glycosidic bond cleavage. Snapshots of one illustrative trajectory are shown in **Figure 6**, which proceeds through the following steps for β-1,4 bond breaking: (B, C) hydrogen transfer between O3 and O5 atoms; (D) C1-O5 bond breaking; (E) β-1,4 bond breaking; and (F) dehydration at C5 atom.

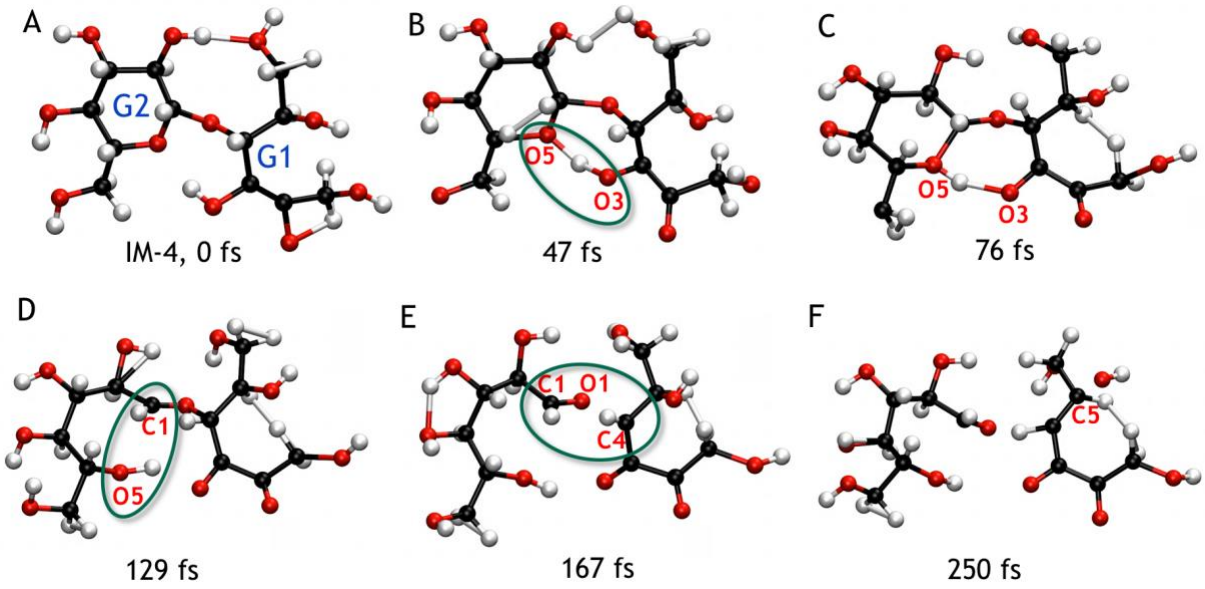

Figure 6. An example of one reactive MD trajectory in which the β-1,4 bond is broken. A) glucose dimer intermediate P3 as shown in Figure 7A; B and C) hydrogen transfer between O3 and O5; D) C1-O5 bond breaking; E) β-1,4 bond breaking; F) C5 dehydration.

Task 2: Quantum mechanical calculations of peeling and pretreatment reactions

Quantum mechanical (QM) calculations were carried out to determine the energy profiles of both wood polysaccharides, cellulose and GGM, under kraft pulping conditions, including primary peeling, stopping, pretreatment, and secondary peeling reactions. These calculations can quantitatively shed light on the fundamental understanding of kraft pulping, the reasons for unexpected loss of GGM even following with MM pretreatment and provide insights for the design of pretreatment agents that can better preserve GGM in kraft pulping.

QM model construction and validation. The dispersion-corrected hybrid meta-GGA density functional approximation M062X-D3[15] and the 6-31G (d,p) basis set were used throughout the study. M062X-D3 was chosen because it is among the top density functionals for calculating conformational energies of carbohydrates,[16] reaction energies for small systems, and noncovalent interactions in the GMTKN55 benchmarks.[17] As an additional evaluation of this model chemistry, we calculated the reaction free energy (ΔG_r) and water-assisted activation free energy (E_a) for the ring opening of cyclic a-D-glucose to form acyclic D-glucose. We obtained ΔG_r = 9.5 kcal/mol at the M062X-D3/6-31g(d,p) level of theory, which is good agreement with the available reference value of 10.3 kcal/mol obtained at the CCSD(T)/G4 level of theory.[18] The calculated value of E_a was 26.6 kcal/mol at M062X-D3/6-31g(d,p), slightly higher than the 23.6 kcal/mol literature reference value calculated at the CBS-QB3 level of theory.[19] Thus, we expect that the M062X-D3/6-31g(d,p) level of theory should provide sufficiently accurate energetics to investigate the model systems in the present work. Initially, we used the SMD polarizable continuum model with water as the solvent to calculate aqueous free energies. However, we found that using this solvent representation resulted in highly inaccurate hydration free energies for small test systems (not shown). Thus, as is commonly done, we included a small number of explicit water molecules to account for explicit hydrogen bonding and to alleviate issues associated with the artificial solute-solvent boundary representation. Similar to the classical MD simulations of dimers, we used a β-(1-4)-glycosidic bonded glucose dimer (Glu-Glu) to represent cellulose and a β-(1-4)-linked mannose dimer (Man-Man) for GGM, respectively, in the QM calculations. All QM calculations were performed with Gaussian 16, revision A.03.[20]

Primary peeling. Alkali-catalyzed endwise degradation, or primary peeling, is the main issue for the loss of non-lignin material during kraft pulping. The generally accepted mechanism of primary peeling is shown in **Figure 7A**. The main steps include: (1) ring opening, (2) aldose-ketose transformation (i.e., enolization), (3) β-elimination, (4) tautomerization, and (5) benzylic acid rearrangement (Sixta, 2006). Our aim is to limit (or ideally, prevent) primary peeling, necessitating a detailed mechanistic understanding of this process. Thus, we calculated a reaction pathway for the primary peeling reactions according to this accepted reaction mechanism. We generated reaction free energy diagrams for these five steps with both Glu-Glu and Man-Man (**Figure 8**).

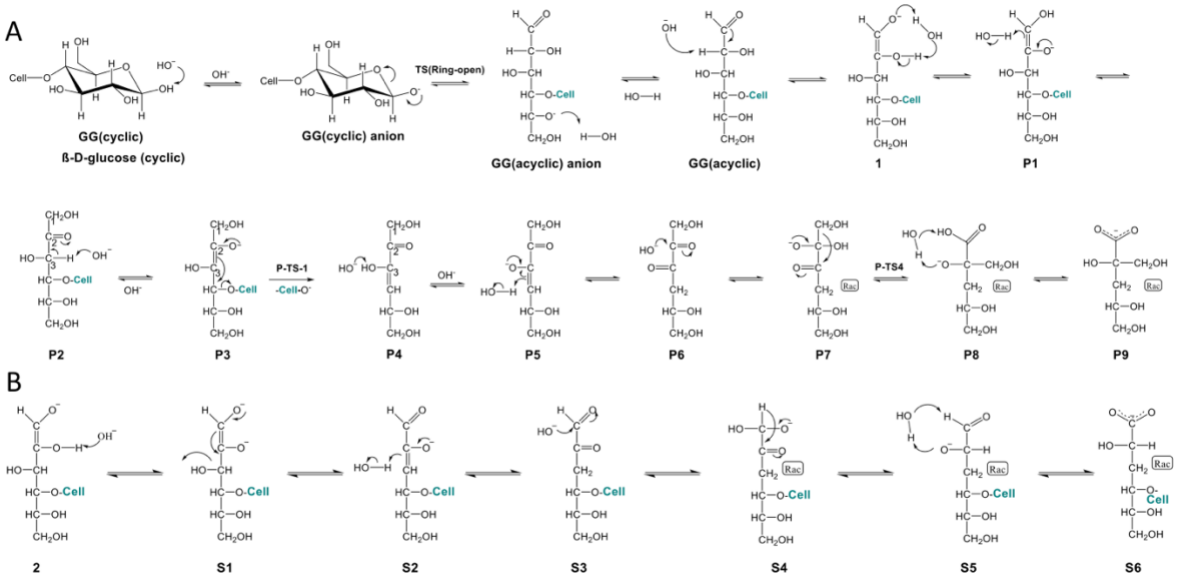

Figure 7. Generally accepted mechanisms for (A) primary peeling (Sixta, 2006) and (B) stopping reactions (Young and Liss, 1978) of the reducing end groups of cellulose during kraft pulping.

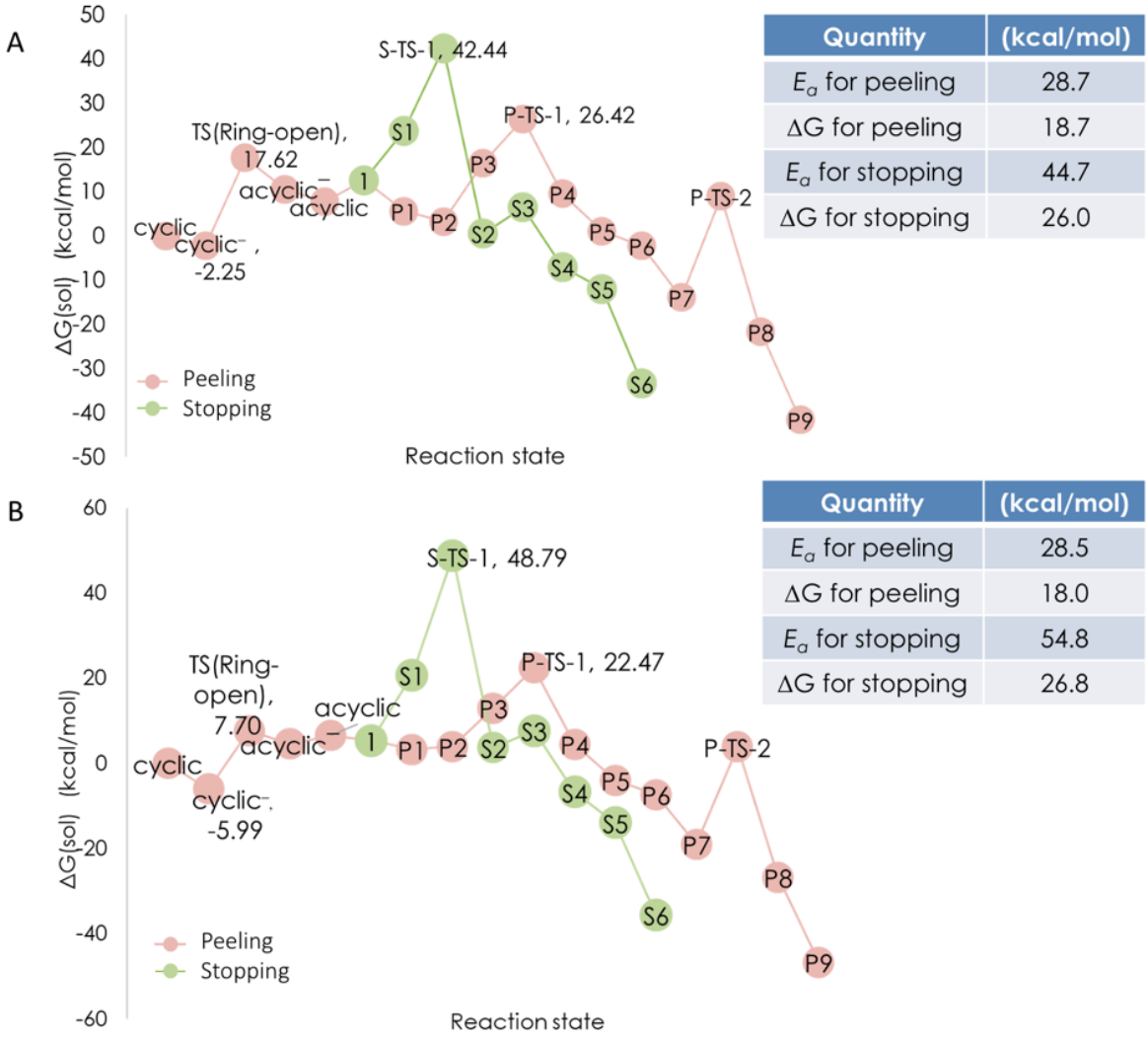

Figure 8. Free energy profiles for peeling and stopping reactions for (A) Glu-Glu (representing cellulose) and (B) Man-Man (representing GGM). Energies of selected high-energy states are shown (kcal/mol). P: peeling, S: stopping. Inset tables report the activation energy (Ea) and free energy difference (ΔGr) for peeling and stopping.

The calculated activation energies (E_a) for primary peeling of the Glu-Glu and Man-Man models are 28.7 and 28.5 kcal/mol, respectively, which can be considered essentially equivalent. These barriers were calculated as the difference in free energy between the low-energy reactant state ("cyclic⁻" in **Figure 8A** or **8B**) and that of the transition state for peeling ("P-TS-1" in **Figure 8A** or **8B**).

Stopping. Stopping reactions (**Figure 7B**) compete energetically with primary peeling reactions (**Figure 7A**) and prevent further sugar loss from a given polysaccharide chain. Consistent with the experimental observations that primary peeling is a significant source of yield loss for both cellulose and GGM, the activation energies for peeling are much lower than those for stopping for both polysaccharides, indicating that many peeling events will occur prior to stopping. The calculated activation energy for stopping is significantly higher (54.8 kcal/mol) for Man-Man than for Glu-Glu (44.7 kcal/mol), indicating that more GGM will be peeled before stopping than will

cellulose. This E_a value was calculated as the difference between the low-energy reactant state ("cyclic" in **Figure 8A** or **8B**) and that of the transition state for stopping ("S-TS-1" in **Figure 8A** or **8B**). We note that the free energy barriers derived from the present DFT calculations are likely not accurate because of limitations of the models. However, the *relative* free energies are more likely to be meaningful due to error cancellation.

Pretreatment. Having examined the intrinsic susceptibility of native (non-pretreated) cellulose and GGM to peeling reactions, we return to the top-level basic research question: *Why does pretreatment with sodium methyl mercaptan increase the pulp yield of cellulose, but not that of GGM*? The first hypothesis we examined is that cellulose undergoes the reaction with methyl mercaptan during pretreatment much more effectively to form stable end groups than does GGM. To test this hypothesis, we proposed the reaction pathway shown in **Figure 9** and calculated the energetics at each structure along the pathway. For the attack of methyl mercaptan upon each polysaccharide, we considered two routes of attack by the thiolate nucleophile, which we refer to as a "bottom-side" and "top-side" attack (**Figure 9B** and **9C**, respectively). The calculated free energies of relevant species along the proposed reaction pathway relative to the are shown in **Table 1**.

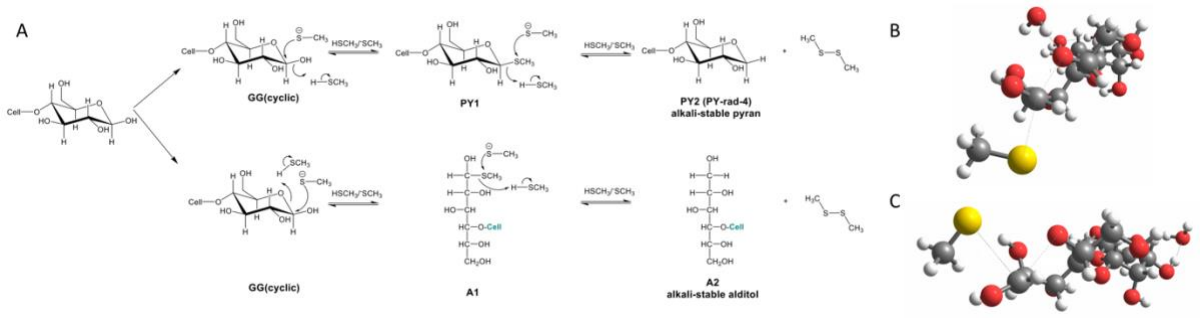

Figure 9. Pretreatment reactions and key intermediates. (A) Proposed mechanism for pretreatment reactions of the reducing end group of Glu-Glu. Geometric arrangement of CH3S- on the Man-Man dimer prior to (B) bottom side and (C) top side attack.

Table 1. Free energies for species within the pretreatment reaction scheme (Figure 9A).

Model[a]	Relative free energy (kcal/mol)	
	Glu-Glu	Man-Man
cyclic	0	0
TS-top	56	66.2
TS-bot	46	38.4
A1(-)	12.0	11.4
A1	-8.2	-8.2
A2	-2.4	-1.3

[a] See **Figure 9**. Note that A1(-) is an anionic version of A1.

These results indicate that alkali-stable reducing end groups (REGs) using MM are formed with similar energy barriers and reaction free energies for both Glu-Glu and Man-Man. Thus, differences in the effectiveness of pretreatment are unlikely to be the primary source of the

different levels of protection observed in previous experiments. Our results indicate that the energy barrier for the pretreatment reaction is *lower* in the case of GGM (38.4 kcal/mol) than it is for cellulose (46 kcal/mol). An alternative hypothesis is that both GGM and cellulose are effectively protected by methanethiolate and form stable end groups, which is supported by our DFT calculations, but that GGM remains more highly susceptible to secondary peeling than cellulose. Secondary peeling involves hydrolysis of an internal glycosidic bond in a polysaccharide chain, thus creating a new chain end.

Secondary peeling (hydrolysis). We calculated a reaction pathway for the generally accepted mechanism of alkaline hydrolysis of Glu-Glu and Man-Man, with a particular emphasis on the energetics of converting the O2-deprotonated species H1 to the epoxide intermediate H2A (**Figure 10A**). We found that intermediate formation is much more favorable for Man-Man than for Glu-Glu (**Table 2**). We attribute this energy difference to the ring conformations of the respective epoxide intermediates. For Man-Man, the intermediate adopts a relatively stable conformation (**Figure 10C**), whereas for the analogous structure for Glu-Glu the intermediate consists of a highly unfavorable conformation (**Figure 10B**). This difference in thermodynamic stability of these two intermediates has the effect of promoting facile hydrolysis of GGM but to a much lesser extent for cellulose. Importantly, hydrolysis creates new REGs. Even though REGs may be protected initially through pretreatment, new REGs that are unprotected may be regenerated during pulping.

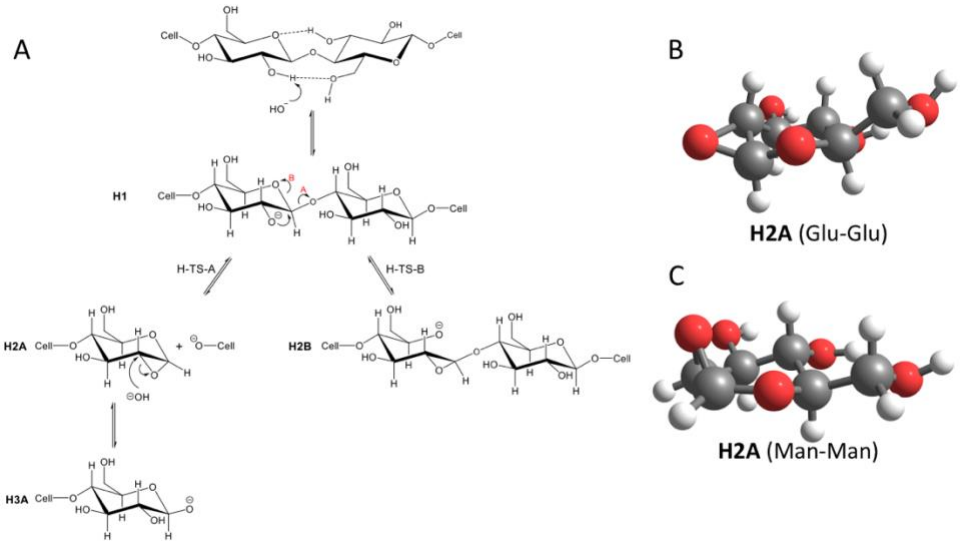

Figure 10. Secondary peeling reaction. (A) Commonly accepted mechanism for secondary hydrolysis reactions (shown for glucose dimer Glu-Glu). (B) Epoxide intermediate structure (H2A in panel (A) for (B) Glu-Glu and (C) Man-Man.

Table 2. Secondary peeling (hydrolysis) free energies corresponding to the structures in Figure 10A.

Modela	Relative free energy (kcal/mol)	
	Glu-Glu	Man-Man
cyclic	0	0
H1 (cyclic-)	-3.7	-1.3
H-TS-A	89.1	52.1
H2A (new REG)	61.3	8.9
H-TS-B	34.0	n/a
H2B	14.0	n/a

a See Figure 10.

Lastly, MD simulations of the cellulose microfibril with GGM molecules described above also may shed some insight into the higher susceptibility of GGM to secondary hydrolysis. **Figure 11** shows the radial distribution for OH^- ions with respect to the glycosidic oxygen (O4) of cellulose and GGM, the site of initiation for secondary peeling. The results indicate a much higher local concentration of OH^- ions around O4 in GGM than cellulose. This effect is likely due to protection provided by the microfibrillar structure of cellulose that is not afforded to GGM.

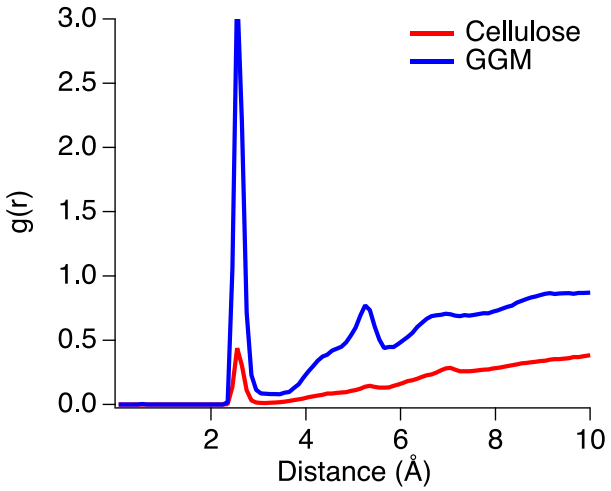

Figure 11. Radial distribution function of OH^- ions at the glycosidic bond (O4 atom) in cellulose and GGM. OH^- ion has much stronger affinity to the O4 atoms in GGM than cellulose, possibly promoting GGM hydrolysis.

We note that some of the free energy barriers calculated with DFT are substantially higher than the corresponding experimental measurements (see below). Although we were still able to gain mechanistic insight into the factors that govern the observed behavior, an obvious future goal would be to improve the agreement between computational results and corresponding experimental values. We suspect that including additional explicit solvent molecules in the DFT calculations will reduce unrealistically high free energy barriers. However, introducing these additional degrees of freedom will substantially increase the computational cost of identifying low

free energy states along the reaction pathways. In addition, other mechanistic hypotheses could be tested to identify energetically more favorable reactions.

Task 3: Experimental kinetic data of real wood chips (University of Maine, Prof. Adriaan van Heiningen)

Pulping experiments were performed using southern pine chips obtained from US mills.

All experiments were performed in quadruplet using four 235 mL cylindrical rocking digesters. About 30 grams of wood chips (on oven dry basis) was used in each digester. In order to avoid the handling of MM gas, an aqueous solution of SMM (21% w/w) containing also a small amount of NaOH (0.4% w/w) with pH 12.9 was obtained from Arkema (King of Prussia, PA 19406). The SMM charge (calculated as MM) was 1 to 6% on wood (oven dry) basis. The liquor-to-wood ratio for MM pre-treatment was 3 L/kg and the pre-treatment temperature was between 80°C to 130°C depending upon the experiment.

At the end of pre-treatment, the digesters were cooled to room temperature (using a water bath) while make-up white liquor was being prepared. The final pH of the pre-treatment liquor was between 9.5 to 10.5. The total liquor-to-wood ratio after adding make-up white liquor was 4.5 L/kg. It should be noted that for some experiments, the SMM solution was charged together with the make-up white liquor to simulate more practical pulp mill conditions. After adding the make-up white liquor (Sulfidity: 30%, Causticization Efficiency: 80%), the digesters were placed in the oil bath for an hour at 115°C to achieve impregnation of white liquor into chips. At the end of impregnation, the digesters were removed from the oil bath and cooled to room temperature while the oil bath was being heated to the cooking temperature of 170°C. The digesters were then immersed in the bath and cooked to target H-factor of about 1960 hrs.

Screened pulp was used for the determination of kappa number (TAPPI Standard T-236) and chemical composition. The carbohydrate composition of wood and pulp was determined using High-Performance Anion Exchange Chromatography (HPAEC) after acid hydrolysis of the pulp sample. TAPPI standard methods (T-249, T-222, and T-204) were used to estimate the composition of lignin and extractives in the wood/pulp samples. The uronic anhydride content was determined using the chromophoric group analysis method developed by Scott.[21] Residual alkali was determined using a modified SCAN-N 2:88 method.

Pre-treatment with 3% MM at 105°C. The initial MM pretreatment experiments were performed at a charge of 3% MM on OD wood at 105°C for 60 minutes. The temperature of 105°C was chosen assuming that at this temperature and a low pH of about 12 of the pretreatment liquor, the kinetics of the primary peeling reactions of GGM and cellulose would be slow enough compared to the kinetics of the reducing end group stabilization reactions of MM.

Figure 12 shows the total pulp yield versus kappa results for the 15% EA control kraft cooks and those with pre-treatment with 3% MM followed by kraft cooking at 15% EA and 12% EA. Since the kappa number for the cook with 3% MM and 15 % EA was about 19, i.e. significantly below the target kappa number of about 25 - 30, a 12% EA cook was performed after pretreatment with 3% MM. In all cases the amount of rejects was negligible at 0.01 - 0.04% on o.d. wood. As expected, there is a linear relationship between total pulp yield and kappa number for the control

cooks. The results clearly show that the addition of MM increased the retention of wood carbohydrates with an increased pulp yield at the same kappa as the control of about 2.5%. It is also important to notice that the 3% MM pretreatment allowed decreasing the EA charge in kraft cooking from 15 to 12% while still achieving the same kappa number as the control kraft cook at 15% EA.

The compositions of the softwood feedstock, 15% EA control kraft pulp, and the 3% MM pretreated followed by 12% EA kraft cook are listed in **Table 3**, all reported based on original dry wood mass. The increased yield of the different components (xylan, GGM, cellulose, and lignin) in the 3% MM pretreated 12% EA kraft pulp compared to the 15% EA control kraft pulp is given at the bottom of the Table. It shows that the increase in the pulp yield is mostly due to the increased retention of cellulose and xylan. It also shows that there is a good agreement between pulp yields calculated from the pulp composition and the measured values. This indicates a good mass balance closure and accurate and reproducible chemical and experimental methods, respectively.

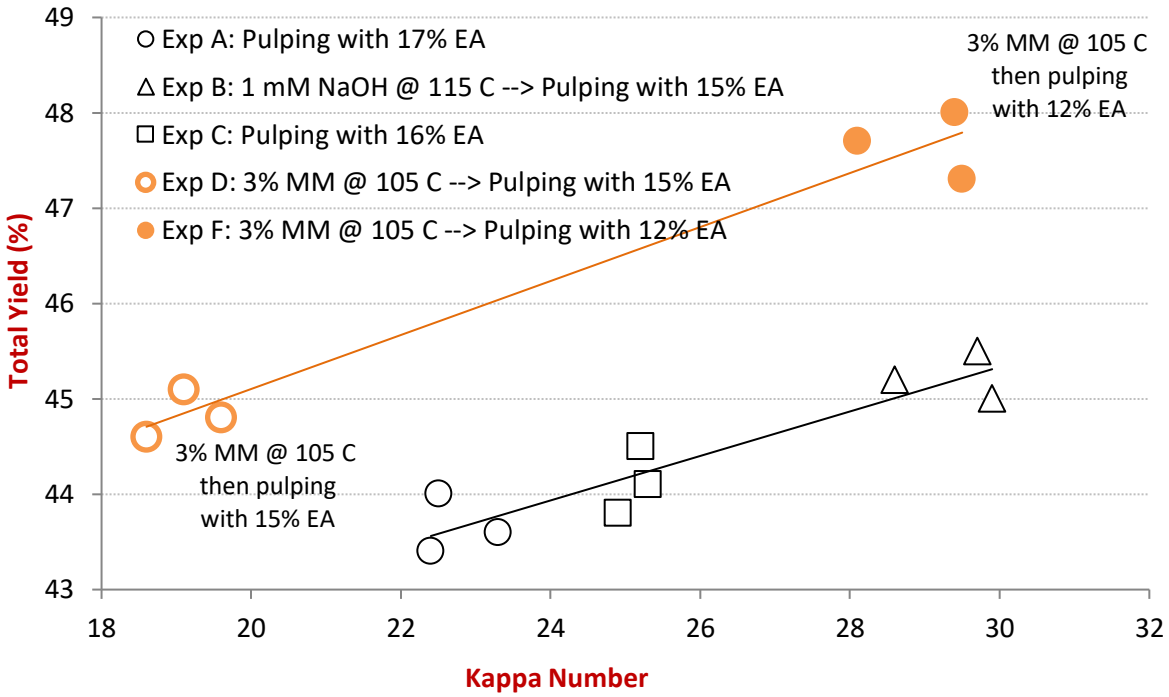

Figure 12. Pre-treatment with 3% MM at 105°C.

Table 3. Composition of Wood and Pulp Samples – Part 1

Sample Type	Composition of wood chips or pulps based on dry wood mass (%)				Pulp yield, based on dry wood mass (%)		Kappa Number
	Xylan	GGM	Cellulose	Lignin	Calculated from pulp analysis data	Measured	
Southern Pine chips	10.28	15.69	41.94	29.5	----	100	----
Control Pulp, 1 mM NaOH @ 115 C → Pulping with 15 % EA	4.42	3.63	34.98	1.86	44.89	45.2	29.4 ± 0.7
3% MM @ 105 C → Pulping with 12 % EA	5.58	3.84	35.87	2.10	47.39	47.7	29.0 ± 0.8
Increased yield with MM (based on dry wood mass)	1.16	0.21	0.89	0.24	2.50	2.50	----

Additional experiments, were conducted to study the effect of various process variable on pulp yield including time, temperature, MM charge, pH, and co-treatment. The details of those experiments were not included here but results are summarized in the conclusions.

Composition of wood and pulp, residual effective alkali, and rejects. **Table 4** lists the percentage increase in the retention of xylan, GGM, cellulose and lignin relative to the control kraft pulp at 15% EA, all expressed on original dry wood mass. Based on these percentages the increase in pulp yield (relative to the yield of the kraft control) is calculated. This calculated pulp yield increase is also listed in **Table 3** together with the measured pulp yield increase. Finally the table includes the kappa number and percentage of rejects and residual alkali content of the final black liquor.

It can be seen that there is good agreement between the calculated and experimentally measured pulp yield increase for most of the experiments. For the experiments with 3% MM, pre-treatment at too high (130°C) temperature resulted in the loss of cellulose, probably due to peeling reactions. Pre-treatment at 115°C resulted in the retention of more cellulose as compared with that of 80°C, which might mean that the stabilization reaction of cellulose by MM at 80°C is too slow to retain additional cellulose. The amount of xylan retention was mostly related to alkali charge because more xylan is dissolved at higher alkaline concentrations. The experiments with pre-treatment at 130°C resulted in a higher retention of xylan presumably because more alkali was consumed by cellulose peeling which in turn lowered the solubility of xylan in the cooking liquor. The amount of GGM retained was very small even for the experiments with pretreatment at 80°C. Since primary peeling of GGM starts at about 80°C,[22] while primary peeling of cellulose is only significant at 130°C[23-24] it may be that MM stabilizes some cellulose before peeling but that the glucomannan stabilization by MM is too slow compared to primary peeling of glucomannan. The residual alkali was generally within the acceptable ranges of 4-10 g/L. Similarly the amount of rejects were less than 0.1% except for two experiments, pre-treatment with 6% MM liquor

followed by pulping with % EA (0.33% rejects) and pre-treatment with 3% MM (pH 10) liquor followed by pulping with 12% EA (0.23% rejects).

When looking at the absolute pulp yield increases one can see that the best condition for MM use is to add it directly to white liquor at a charge of 3% (w/w) on wood (as MM). It is hypothesized that the MM stabilization reaction of cellulose occurs during the 60 minutes impregnation phase at 115°C, but unfortunately the stabilization reaction of GGM by MM is too slow compared to the GGM primary peeling reaction to affect the retention of GGM.

Table 4. Composition of pulp samples, rejects, and residual alkali.

Sample Type	Actual composition (for 15% EA control pulp) OR increase in the composition (for remaining samples) relative to control pulp, based on dry wood mass (%)				Increase in the pulp yield, based on dry wood mass (%)		Kappa Number	Rejects (%)	Residual effective alkali (g/L Na_2O)
	Xylan	GGM*	Cellulose	Lignin	Calculated from pulp analysis data	Measured from pulp yield data			
1 mM NaOH @115 C -> Pulping with 15% EA	4.42	3.63	34.98	1.86	----	------	29.4 ± 0.7	0.04 ± 0.02	7.7 ± 0.15
Pulping with 16 % EA	0.19	-0.03	-1.09	-0.35	-1.29	-1.10	25.1 ± 0.2	0.05 ± 0.00	9.3 ± 0.20
Pulping with 17 % EA	-0.04	-0.11	-0.71	-0.55	-1.42	-1.50	22.7 ± 0.5	0.06 ± 0.05	10.6 ± 0.20
3% MM @ 105 C -> Pulping with 15% EA	0.41	0.28	-0.61	-0.39	-0.32	-0.40	19.1 ± 0.5	0.03 ± 0.02	9.5 ± 0.68
3% MM @ 105 C -> Pulping with 12% EA	1.16	0.21	0.89	0.24	2.49	2.50	29.0 ± 0.8	0.01 ± 0.01	6.2 ± 0.04
3% MM @ 115 C -> Pulping with 12% EA	0.88	0.12	1.84	0.06	2.90	2.90	30.0 ± 0.5	0.04 ± 0.00	5.6 ± 0.06
3% MM, pH 12, @ 130 C -> Pulping w/ 12%EA	1.25	0.16	-0.11	0.38	1.67	2.10	29.7 ± 0.9	0.01 ± 0.01	5.8 ± 0.08
3% MM + 12% EA (@ 80 C, 90 mins.) pulping w/o impregnation	0.80	0.54	0.68	0.23	2.24	2.20	28.8 ± 2.1	0.05 ± 0.01	6.0 ± 0.10
6% MM @ 80 C, 90 mins. -> Pulping w/11%EA	1.13	0.13	0.03	0.16	1.44	1.40	26.3 ± 0.5	0.04 ± 0.03	6.4 ± 0.15
3% MM, pH 10, @ 130 C -> Pulping w/12% EA	1.60	0.35	0.93	1.83	4.70	4.80	46.6 ± 1.3	0.23 ± 0.04	3.3 ± 0.23
1% MM @ 115 C -> Pulping with 14% EA	0.64	0.02	-0.05	0.03	0.63	0.60	26.5 ± 0.4	0.00 ± 0.00	7.0 ± 0.13
6% MM @ 115 C -> Pulping with 9% EA	1.78	0.46	2.17	1.34	5.74	5.80	40.1 ± 0.8	0.33 ± 0.05	4.3 ± 0.01
6% MM @ 115 C -> Pulping with 11% EA	1.17	0.12	1.84	-0.21	2.92	2.90	25.9 ± 0.3	0.02 ± 0.00	6.5 ± 0.15
Pulping with 3% MM and 12% EA together	0.69	0.26	1.58	0.10	2.63	2.60	27.5 ± 0.4	0.03 ± 0.02	6.2 ± 0.22
Pulping with 6% MM and 10% EA together	1.27	-0.04	1.24	0.22	2.68	2.70	29.6 ± 1.4	0.12 ± 0.17	5.6 ± 0.22

* GGM = Galactoglucomannan

In summary, the results from a variety of molecular modeling techniques indicate several key findings. Classical MD simulations of biomass polysaccharides cellulose and GGM indicate that OH^- ions have a greater tendency to bind to the reducing end of GGM than cellulose, suggesting that the crystalline nature of cellulose may render a physical protection against peeling. MD simulations of glucose and mannose dimers (representing cellulose and GGM, respectively) demonstrate an enhanced occurrence of hydroxide ions in regions that could promote peeling in GGM, even when the end group is converted to an alkali-stable chemical functionality. DFT results indicate that, although the peeling reactions have similar energetic profiles for the glucose and mannose dimers, the stopping reaction presents a much higher barrier in the case of the mannose dimer, indicating that, once initiated, more successive peeling events will occur for GGM before stopping than in cellulose. Importantly, DFT results indicate that alkali-stable reducing end groups formed via MM pretreatment are formed with similar energy barriers in the two polysaccharides, indicating that pretreatment effectiveness is unlikely to be the primary source for the different levels of protection observed experimentally. Lastly, our calculations indicate that GGM is much more susceptible to internal hydrolysis of a carbohydrate linkage than cellulose (regardless of pretreatment). This internal chain scission is important because it leads to the creation of a new chain end, which can subsequently be depolymerized, a phenomenon known as secondary peeling. Thus, even though reducing end groups may be protected initially through pretreatment, new (unprotected) reducing end groups may be regenerated during pulping. If secondary hydrolysis is the primary mechanism for GGM yield loss, it is possible that co-treatment with MM during kraft pulping could be carried out to cap newly created REGs as they form through secondary peeling. Experimentally, pre-treatment with 3% MM resulted in about 2.5% increase in the pulp yield, and this may be close to the optimal MM loading, given that pre-treatment with 6% MM produced diminishing results and the use of 1% did not lead to a significant yield increase.

References:

1. Negahdar, L.; Delidovich, I.; Palkovits, R., Aqueous-phase hydrolysis of cellulose and hemicelluloses over molecular acidic catalysts: Insights into the kinetics and reaction mechanism. *Applied catalysis B: environmental* **2016,** *184*, 285-298.
2. Jorgensen, W. L.; Chandrasekhar, J.; Madura, J. D.; Impey, R. W.; Klein, M. L., Comparison of simple potential functions for simulating liquid water. *The Journal of chemical physics* **1983,** *79*, 926-935.
3. MacKerell, A. D.; Brooks, B.; Brooks, C. L.; Nilsson, L.; Roux, B.; Won, Y.; Karplus, M., CHARMM: the energy function and its parameterization. *Encyclopedia of computational chemistry* **1998**.
4. Guvench, O.; Greene, S. N.; Kamath, G.; Brady, J. W.; Venable, R. M.; Pastor, R. W.; Mackerell, A. D., Additive empirical force field for hexopyranose monosaccharides. *Journal of computational chemistry* **2008,** *29*, 2543-2564.
5. Hatcher, E. R.; Guvench, O.; MacKerell Jr, A. D., CHARMM additive all-atom force field for acyclic polyalcohols, acyclic carbohydrates, and inositol. *Journal of chemical theory and computation* **2009,** *5*, 1315-1327.
6. Hynninen, A. P.; Crowley, M. F., New faster CHARMM molecular dynamics engine. *Journal of computational chemistry* **2014,** *35*, 406-413.

7. Kräutler, V.; Van Gunsteren, W. F.; Hünenberger, P. H., A fast SHAKE algorithm to solve distance constraint equations for small molecules in molecular dynamics simulations. *Journal of computational chemistry* **2001,** *22*, 501-508.
8. Darden, T.; York, D.; Pedersen, L., Particle mesh Ewald: An N· log (N) method for Ewald sums in large systems. *The Journal of chemical physics* **1993,** *98*, 10089-10092.
9. Van Duin, A. C.; Dasgupta, S.; Lorant, F.; Goddard, W. A., ReaxFF: a reactive force field for hydrocarbons. *The Journal of Physical Chemistry A* **2001,** *105*, 9396-9409.
10. Senftle, T. P.; Hong, S.; Islam, M. M.; Kylasa, S. B.; Zheng, Y.; Shin, Y. K.; Junkermeier, C.; Engel-Herbert, R.; Janik, M. J.; Aktulga, H. M., The ReaxFF reactive force-field: development, applications and future directions. *npj Computational Materials* **2016,** *2*, 15011.
11. Han, Y.; Jiang, D.; Zhang, J.; Li, W.; Gan, Z.; Gu, J., Development, applications and challenges of ReaxFF reactive force field in molecular simulations. *Frontiers of Chemical Science and Engineering* **2016,** *10*, 16-38.
12. Rahnamoun, A.; Van Duin, A., Reactive molecular dynamics simulation on the disintegration of Kapton, POSS polyimide, amorphous silica, and teflon during atomic oxygen impact using the ReaxFF reactive force-field method. *The Journal of Physical Chemistry A* **2014,** *118*, 2780-2787.
13. Monti, S.; Corozzi, A.; Fristrup, P.; Joshi, K. L.; Shin, Y. K.; Oelschlaeger, P.; van Duin, A. C.; Barone, V., Exploring the conformational and reactive dynamics of biomolecules in solution using an extended version of the glycine reactive force field. *Physical Chemistry Chemical Physics* **2013,** *15*, 15062-15077.
14. Monti, S.; Li, C.; Carravetta, V., Reactive dynamics simulation of monolayer and multilayer adsorption of glycine on Cu (110). *The Journal of Physical Chemistry C* **2013,** *117*, 5221-5228.
15. Zhao, Y.; Truhlar, D. G., The M06 suite of density functionals for main group thermochemistry, thermochemical kinetics, noncovalent interactions, excited states, and transition elements: two new functionals and systematic testing of four M06-class functionals and 12 other functionals. *Theoretical Chemistry Accounts* **2008,** *120*, 215-241.
16. Marianski, M.; Supady, A.; Ingram, T.; Schneider, M.; Baldauf, C., Assessing the Accuracy of Across-the-Scale Methods for Predicting Carbohydrate Conformational Energies for the Examples of Glucose and α-Maltose. *Journal of Chemical Theory and Computation* **2016,** *12*, 6157-6168.
17. Goerigk, L.; Hansen, A.; Bauer, C.; Ehrlich, S.; Najibi, A.; Grimme, S., A look at the density functional theory zoo with the advanced GMTKN55 database for general main group thermochemistry, kinetics and noncovalent interactions. *Physical Chemistry Chemical Physics* **2017,** *19*, 32184-32215.
18. Assary, R. S.; Curtiss, L. A., Comparison of Sugar Molecule Decomposition through Glucose and Fructose: A High-Level Quantum Chemical Study. *Energy & Fuels* **2012,** *26*, 1344-1352.
19. Seshadri, V.; Westmoreland, P. R., Concerted reactions and mechanism of glucose pyrolysis and implications for cellulose kinetics. *The Journal of Physical Chemistry A* **2012,** *116*, 11997-12013.
20. Frisch, M. J.; Trucks, G. W.; Schlegel, H. B.; Scuseria, G. E.; Robb, M. A.; Cheeseman, J. R.; Scalmani, G.; Barone, V.; Petersson, G. A.; Nakatsuji, H.; Li, X.; Caricato, M.; Marenich, A. V.; Bloino, J.; Janesko, B. G.; Gomperts, R.; Mennucci, B.; Hratchian, H. P.; Ortiz, J. V.;

Izmaylov, A. F.; Sonnenberg, J. L.; Williams; Ding, F.; Lipparini, F.; Egidi, F.; Goings, J.; Peng, B.; Petrone, A.; Henderson, T.; Ranasinghe, D.; Zakrzewski, V. G.; Gao, J.; Rega, N.; Zheng, G.; Liang, W.; Hada, M.; Ehara, M.; Toyota, K.; Fukuda, R.; Hasegawa, J.; Ishida, M.; Nakajima, T.; Honda, Y.; Kitao, O.; Nakai, H.; Vreven, T.; Throssell, K.; Montgomery Jr., J. A.; Peralta, J. E.; Ogliaro, F.; Bearpark, M. J.; Heyd, J. J.; Brothers, E. N.; Kudin, K. N.; Staroverov, V. N.; Keith, T. A.; Kobayashi, R.; Normand, J.; Raghavachari, K.; Rendell, A. P.; Burant, J. C.; Iyengar, S. S.; Tomasi, J.; Cossi, M.; Millam, J. M.; Klene, M.; Adamo, C.; Cammi, R.; Ochterski, J. W.; Martin, R. L.; Morokuma, K.; Farkas, O.; Foresman, J. B.; Fox, D. J. *Gaussian 16 Rev. C.01*, Wallingford, CT, 2016.

21. Scott, R. W., Colorimetric determination of hexuronic acids in plant materials. *Analytical chemistry* **1979,** *51*, 936-941.

22. Montagna, P. N.; Inalbon, M. C.; Paananen, M.; Sixta, H.; Zanuttini, M. A., Diffusion dynamics in Pinus sylvestris Kraft impregnation: effect of deacetylation and galactoglucomannan degradation. *Industrial & Engineering Chemistry Research* **2013,** *52*, 3658-3662.

23. Nieminen, K.; Paananen, M.; Sixta, H., Kinetic model for carbohydrate degradation and dissolution during kraft pulping. *Industrial & Engineering Chemistry Research* **2014,** *53*, 11292-11302.

24. Paananen, M.; Tamminen, T.; Nieminen, K.; Sixta, H., Galactoglucomannan stabilization during the initial kraft cooking of Scots pine. *Holzforschung* **2010,** *64*, 683-692.

Subject Inventions Listing:

None

ROI #:

None